AVERAGE PLASMA ENVIRONMENT AT GEOSYNCHRONOUS ORBIT

S.-Y. Su
Lockheed Electronics Co., Inc.

A. Konradi
NASA Johnson Space Center

SUMMARY

The average plasma environment at geosynchronous orbit (GSO) is derived from a whole year's worth of plasma data obtained by the UCSD electrostatic electrometer on board ATS-5. The result is primarily intended for use as a general reference for engineers designing a large spacecraft to be flown at GSO. A simple mathematical formula using a 3rd order polynomial is found to be adequate for representing the yearly averaged particle energy spectrum from 70 to 41,000 eV under different geomagnetic conditions. Furthermore, correlation analyses with the geomagnetic planetary index Kp and with the auroral electrojet index AE were carried out in the hope that the ground observations of the geomagnetic field variations can be used to predict the plasma variations in space. Unfortunately, the results indicate that such forecasting is not feasible by use of these two popular geomagnetic parameters alone.

INTRODUCTION

A general introduction to the plasma environment near geosynchronous orbit (GSO) was given by S. E. DeForest (ref. 1) at last year's conference. It was understood that the dynamic behavior of the plasma environment near GSO is extremely complicated and that the observations made by a single spacecraft so far fail to resolve the temporal and spatial variations of the environment. Without complete knowledge of the physical processes of the environment, it is impossible to present any numerical model to quantify the plasma parameters that describe the complicated dynamic magnetosphere during the substorm period. However, long-term statistical averages of the plasma environment can be used as a ground-zero approach in defining the plasma environment at GSO. Such a model can be used by theoreticians as the steady-state solution in the particle-spacecraft interaction model. It also is a great asset to engineers in understanding the long-term dosage of the low radiation to be considered in the design of a large spacecraft.

Only a few spacecraft have carried detectors that are capable of measuring particles with a wide range of energies. The UCSD plasma experiment flown on ATS-5 at GSO measured plasma energy flux intensity for the energy range from 50 to 50,000 eV for both positive ions (assumed to be protons) and electrons. These particle data represent the typical plasma environment at GSO. They are available to the science community in the form of particle energy spectrograms plotted on microfilm, with differential energy flux intensities encoded into a range of gray scales. No example of such a spectrogram will be shown here because it is assumed that the audience is familiar

with the format of McIlwain's spectrogram (ref. 2). The data coverage was fairly complete at the beginning of experiment so that the year 1970 was chosen for long-term statistical analysis. The year 1970 is quite close to the sun-spot maximum of the 11-year solar cycle; thus, these plasma data should represent a moderately active radiation environment at GSO.

DATA REDUCTION

To obtain the numerical values of the particle energy spectrum for the present analysis, we first used the Boller and Chivens Photometric Data System's Microdensitometer to digitize the gray codings of the energy flux intensity in the spectrogram from the microfilm. In order to avoid edge-interference of the data on the microfilm during the process of digitization, the minimum and maximum energy limits are set at 70 eV and 41,000 eV, respectively. Forty-eight energy level steps between the minimum and maximum limits were chosen to cover approximately equal energy intervals on a logarithmic scale. The data were digitized at 10-minute spacings of universal time (UT). The numerical data of day 1 and day 2 of 1970 obtained by the digitization procedure were plotted to compare with the data published by DeForest and McIlwain (ref. 2). The digitized data were found to be accurate within a factor of 2 of the original data. The digitized particle energy flux intensities were converted to particle number flux intensities by dividing the energy flux intensities by the corresponding energy level measured in eV. The data for each 10-minute interval is then stored as a single data point in the computer's memory to create a large data bank for the analysis carried out in the next section.

Owing to the man-power shortage for digitizing the spectrogram on the microfilm, only the particle fluxes perpendicular to the local geomagnetic field lines were digitized. The pitch angle distributions of the particles are not available in the present analysis.

DATA ANALYSIS

The data are presented in local time (LT), instead of universal time (UT), to indicate the satellite location in the magnetosphere. The local time is related to universal time by the formula LT = UT-7. As mentioned before, the data are obtained at 10-minute intervals and are stored in the computer's memory bank. Three consecutive data points are then averaged into one half-hour data point. All available half-hour averages in 1970 were then averaged into 24 hourly averaged data points along the satellite's 24-hour period orbit. The results are shown in Figure 1. The electrons are seen to have higher flux intensities than the protons at all times. The shapes of the energy spectra for both protons and electrons change very little between two adjacent local-time observations. However, noticeable changes are evident in the flux intensities and in spectral shapes between widely separated local times (e.g., compare 00-01 LT and 12-13 LT). The reason for such differences is that the satellite detects large flux intensities in the night-side magnetosphere where the low energy plasmas are energized during substorms. As those newly energized plasmas begin to drift around the earth toward the day-side magnetosphere, they are subjected to various loss mechanisms and to particle

dispersion effects. Thus, they appear to be different in spectral shape and in intensity level when they are detected by the spacecraft on the day-side or on the night-side. The observation of a local minimum in both the proton and electron spectra for the energy range from 500 to 8000 eV, in the day-side magnetosphere, indicates that both particle species in that energy range have been greatly depleted due to a greater loss process operative on them.

The results of the averaged, energy-integrated number flux, energy flux, and energy density of low energy plasma particles observed in 1970 are listed in Tables 1 and 2 for protons and electrons, respectively. It is known from experience that protons and electrons with energies between 10,000 and 200,000 eV contribute substantially to energy flux intensity and energy density, but not to number flux intensity. Since the present study covers only particle energies up to 41,000 eV, to obtain estimates of the particle energy flux and the energy density at GSO we should multiply the values given in Tables 1 and 2 by factors of 2 to 5.

A frequency distribution of the occurrence of large integral flux levels along the satellite orbit is plotted in Figure 2. The criteria for selecting the critical flux levels for protons and electrons are set so that they represent flux intensities that are commonly observed during moderate substorms. The high electron flux intensities are primarily observed in the night-side magnetosphere, with the maximum frequency occurrence located between 01 and 02 LT. On the other hand, high proton flux intensities are observed at all local times although the peak frequency is still centered around 00 LT. The reason for such contrast in distribution is that the electrons are more readily precipitated into the upper atmosphere as they drift toward the day-side magnetosphere after they are injected in the night-side magnetosphere; thus, they rarely show high flux levels on the day-side. Protons, on the other hand, are more stable so that the level of flux intensity is more or less maintained along the drift paths after they were injected in the night-side magnetosphere.

Because the loss mechanism is not very operative for protons, the level of proton flux intensity along the GSO changes very little, indicating lesser dependence on geomagnetic conditions, while the electron flux intensity fluctuates drastically in accordance with geomagnetic activities. In other words, the maximum and minimum electron flux intensities can differ by about a factor of 750, yet the maximum and minimum proton flux intensities differ merely by a factor of 20.

One of the objectives of the present data analysis is to correlate the energy-integrated flux intensities observed at GSO with the geomagnetic activities represented by some types of ground observations. This is carried out in the hope that the total flux level in space can be predicted from observations of geomagnetic indices on the ground. Because of the different loss mechanisms operative upon protons and electrons at GSO, the measured electron flux intensities may fail to show any large flux variations in the day-side magnetosphere as seen in Figure 2. On the other hand, the newly injected protons may blend with the old residual proton fluxes and drift together around the earth to become indistinguishable from each other. The complicated temporal and spatial variations of the protons and electrons in space may limit the utility of the

correlation analysis. Nevertheless, a linear correlation analysis was carried out to determine the degree of the relationship between the particle flux intensities and the geomagnetic indices. The geomagnetic indices used for the analysis are the auroral electrojet (AE) index and the geomagnetic planetary (Kp) index. The AE index can, in principle, reveal substorm activity in the magnetosphere and is available in half-hour averages for the present study. On the other hand, the Kp index is only available in 3-hour averages so that correlation analysis with this index is carried out for supplementary purposes only. The linear correlation coefficients for the electron and proton fluxes with AE indices at various lag times are shown in Figure 3. The correlation analysis was carried out by using logarithmic values of the flux intensities and the AE values. Analyses with different combinations in the form of the flux intensities and the AE indices were also performed. No significant changes in linear correlation coefficients were noticed so that Figure 3 can be regarded as a typical result.

As was expected, a correlation between the particle flux intensity in space and the AE index observed on the ground exists, but is not as striking as one might anticipate. Although the correlation coefficient is barely larger than 0.2 as shown in Figure 3, the probability of having 15,000 random pairs of numbers for a correlation coefficient of 0.2 is much less than 0.0001 (Bevington, ref. 3). Therefore, a definite, causal relationship does exist between the observation of high particle flux intensity in space and recordings of the large AE values by ground stations. However, the low correlation coefficient also indicates that we cannot expect a one-to-one correspondence between the variations of the flux intensity and the AE index. In general, the correlation coefficients between the electron flux intensities and the AE indices are better than those between proton flux intensities and the AE indices, but still lack any striking significance. Since the particles are most likely to be energized in the night-side magnetosphere and therefore show high flux intensities during substorms, there may exist a better correlation between particle fluxes and the substorm indicator index AE during the 12-hour period each day when the satellite is in the night-side magnetosphere. Therefore, we have calculated another correlation coefficient between the electron flux variations and the AE indices in regions of local time from 20 LT through midnight to 08 LT. This coincides with the regions of high probability for observing large electron flux intensity as seen in Figure 2. The result is shown in Figure 4. The correlation coefficients are impressively high. The peak correlation occurs with the AE index shifted half an hour ahead in time of the observed electron flux intensity. The peak coefficient of 0.65 implies that there is probably a one-to-one correspondence between the peaks of the AE index and the electron flux intensity. With the best correlation being obtained by comparing the flux intensity with the AE index half an hour before the flux observation, we might think that we could forecast the arrival of a large electron flux at the spacecraft. However, the slow changes in the correlation coefficients around the peak value as seen in Figure 4 means that the prediction may be impractical because of the lack of definite cut-off criteria for selecting the peak.

The proton fluxes, on the other hand, fail to show an improved correlation with the AE index even when the satellite observation is limited to the night-side magnetosphere so that we did not plot the results in Figure 4.

Furthermore, neither proton nor electron fluxes show a good correlation with the Kp indices. Since the Kp index can now be forecasted on a real-time basis, as a reference to the expected values of the particle flux intensities at different Kp values, Table 3 lists the maximum particle flux intensities observed at various local times for different Kp values. The particle flux intensity, in general, increases as Kp increases. However, there are some flux intensities which are observed during very high Kp yet show smaller values than those observed at lower Kp as seen in Table 3. The reason for such a discrepancy is due to the fact that the number of observations made during high Kp is too small to yield a good statistical representation.

MATHEMATICAL MODEL

Another objective of the data analysis is to derive a mathematical model for particle flux intensities observed at GSO. The model can be used for simulation of particle encounters by a spacecraft at a certain local time with a specified geomagnetic condition. However, we should always remember that the dynamic behavior of the plasmas at GSO is so complicated that only the statistical averages of the particle fluxes can be predicted.

From inspection of Figure 1, we conclude that the particle energy spectrum cannot be fitted by a single Maxwellian distribution function, but a reasonably good fit may be obtained by a composite of several Maxwellian distributions. The search for correct components in the optimum set of the composite functions can become a very tedious and laborious process. Since the use of composite functions may bear no physical significance with respect to the actual particle flux distribution, we may as well use a polynomial curve to fit the particle flux intensity. We selected polynomials varying from 1st to 10th order to carry out the least-squares procedure for fitting all the flux intensities in Figure 1. The chi-square test is then applied to choose the best-fit polynomial. It was found that a 3rd order polynomial yields a consistently low value of chi-square. On this basis, we conclude that the 3rd order polynomial can best represent the flux intensities in Figure 1.

The result of the polynomial fit is given by...

$$\log_{10}(F) = A_1 + A_2(\log_{10} E) + A_3(\log_{10} E)^2 + A_4(\log_{10} E)^3 \qquad (1)$$

where F is the particle number flux intensity and E is the particle energy in eV. The coefficients A_1 through A_4 have also been evaluated for different local times and geomagnetic conditions. Tables 4 through 6 show values of these coefficients for the model applied at the given local time under a specific geomagnetic condition. The value of the particle flux intensity calculated from Equation (1) is of course valid only for the particle energy range from 70 to 41,000 eV.

REFERENCES

1. DeForest, S.E.: The Plasma Environment at Geosynchronous Orbit, Proceedings of the Spacecraft Charging Technology Conference, AFGL-TR-77-0051, 1977, pp. 37-52.
2. DeForest, S.E.; McIlwain, C.E.: Plasma Clouds in the Magnetosphere, Journal of Geophysical Research, 1971, pp. 3587-3611.
3. Bevington, P.R.: Data Reduction and Error Analysis for the Physical Sciences, McGraw-Hill Book Co., New York, 1969, pp. 119-163.

TABLE 1. Protons at Geostationary Altitude

Local Time	Flux Intensity protons/cm^2-sec-ster	Energy Density ergs/cm^3-ster	Energy Flux Intensity ergs/cm^2-sec-ster
00-01	1.14 E 7	1.48 E-9	0.278
01-02	1.08 E 7	1.40 E-9	0.268
02-03	1.34 E 7	1.45 E-9	0.268
03-04	1.45 E 7	1.54 E-9	0.291
04-05	1.00 E 7	1.17 E-9	0.222
05-06	9.01 E 6	1.12 E-9	0.215
06-07	8.47 E 6	1.09 E-9	0.212
07-08	7.83 E 6	1.03 E-9	0.203
08-09	7.39 E 6	9.96 E-10	0.200
09-10	7.08 E 6	9.88 E-10	0.203
10-11	7.13 E 6	1.02 E-9	0.210
11-12	7.29 E 6	1.06 E-9	0.218
12-13	7.55 E 6	1.12 E-9	0.231
13-14	8.12 E 6	1.21 E-9	0.249
14-15	8.60 E 6	1.28 E-9	0.259
15-16	9.16 E 6	1.37 E-9	0.278
16-17	1.00 E 7	1.45 E-9	0.290
17-18	1.10 E 7	1.59 E-9	0.316
18-19	1.10 E 7	1.59 E-9	0.315
19-20	1.10 E 7	1.57 E-9	0.310
20-21	1.14 E 7	1.61 E-9	0.315
21-22	1.15 E 7	1.61 E-9	0.315
22-23	1.17 E 7	1.61 E-9	0.312
23-24	1.16 E 7	1.55 E-9	0.295

TABLE 2. Electrons at Geostationary Altitude

Local Time	Flux Intensity electrons/cm^2-sec-ster	Energy Density ergs/cm^3-ster	Energy Flux Intensity ergs/cm^2-sec-ster
00-01	2.90 E 8	5.47 E-10	3.03
01-02	3.49 E 8	6.76 E-10	3.87
02-03	3.41 E 8	6.69 E-10	3.85
03-04	3.26 E 8	6.55 E-10	3.89
04-05	3.44 E 8	6.07 E-10	3.61
05-06	2.73 E 8	5.43 E-10	3.24
06-07	2.39 E 8	4.81 E-10	2.93
07-08	1.98 E 8	4.07 E-10	2.54
08-09	1.56 E 8	3.26 E-10	2.06
09-10	1.21 E 8	2.54 E-10	1.65
10-11	1.01 E 8	2.14 E-10	1.41
11-12	8.38 E 7	1.78 E-10	1.18
12-13	6.97 E 7	1.53 E-10	1.02
13-14	6.45 E 7	1.42 E-10	0.952
14-15	5.88 E 7	1.28 E-10	0.856
15-16	5.52 E 7	1.18 E-10	0.787
16-17	5.89 E 7	1.21 E-10	0.798
17-18	5.35 E 7	1.01 E-10	0.638
18-19	5.69 E 7	1.01 E-10	0.614
19-20	6.66 E 7	1.10 E-10	0.629
20-21	9.90 E 7	1.66 E-10	0.907
21-22	1.47 E 8	2.55 E-10	1.41
22-23	1.95 E 8	3.38 E-10	1.79
23-24	2.44 E 8	4.38 E-10	2.34

TABLE 3A. Maximum Proton Integral Fluxes
(Protons/cm^2-sec-ster)

K_p / UT*	0-2	2+-4	4+-6	6+-9
00-03	1.08E7	1.39E7	1.93E7	1.59E7
03-06	1.19E7	1.46E7	1.83E7	2.10E7
06-09	1.22E7	1.56E7	1.64E7	2.38E7
09-12	1.00E7	1.27E7	1.93E7	8.17E6
12-15	8.36E6	1.05E7	1.83E7	1.47E7
15-18	7.25E6	9.59E6	1.73E7	1.18E7
18-21	7.98E6	1.02E7	1.51E7	7.23E6
21-24	9.51E6	1.21E7	1.69E7	2.12E7

*LT = UT-7

TABLE 3B. Maximum Electron Integral Fluxes
(Electrons/cm^2-sec-ster)

K_p / UT*	0-2	2+-4	4+-6	6+-9
00-03	5.43E7	8.49E7	3.30E8	3.91E8
03-06	1.12E8	3.58E8	5.54E8	9.49E8
06-09	3.22E8	5.86E8	9.23E8	1.08E9
09-12	3.20E8	6.37E8	8.65E8	8.17E8
12-15	2.04E8	4.50E8	7.65E8	6.89E8
15-18	1.18E8	2.31E8	4.88E8	1.73E8
18-21	8.27E7	1.08E8	1.23E8	5.25E7
21-24	7.59E7	6.89E7	8.05E7	2.46E8

*LT = UT-7

TABLE 4. Coefficients of the polynomial fit to the yearly averaged fluxes

	LT	A_1	A_2	A_3	A_4
Protons	00-01	7.193	-3.491	-0.976	-0.099
	01-02	8.039	-4.177	1.148	-0.113
	02-03	7.216	-3.276	0.850	-0.082
	03-04	6.431	-2.465	0.572	-0.052
	04-05	6.103	-2.019	0.414	-0.035
	05-06	5.707	-1.500	0.222	-0.014
	06-07	5.554	-1.329	0.146	-0.004
	07-08	4.982	-0.705	-0.007	0.021
	08-09	3.763	0.519	-0.495	0.067
	09-10	3.641	0.869	-0.673	0.091
	10-11	3.748	0.782	-0.670	0.094
	11-12	5.008	-0.385	-0.349	0.067
	12-13	6.788	-2.108	0.161	0.019
	13-14	8.502	-3.954	0.758	-0.041
	14-15	10.529	-6.041	1.439	-0.112
	15-16	12.002	-7.589	1.953	-0.165
	16-17	11.561	-7.238	1.903	-0.167
	17-18	13.097	-8.940	2.486	-0.229
	18-19	13.565	-9.370	2.616	-0.241
	19-20	11.908	-7.944	2.220	-0.206
	20-21	12.424	-8.415	2.377	-0.223
	21-22	11.050	-7.099	1.986	-0.186
	22-23	10.313	-6.351	1.770	-0.167
	23-24	8.962	-5.202	1.475	-0.144
Electrons	00-01	9.789	-5.258	1.892	-0.237
	01-02	8.721	-3.981	1.446	-0.187
	02-03	9.550	-4.797	1.699	-0.212
	03-04	9.417	-4.599	1.595	-0.197
	04-05	9.470	-4.578	1.565	-0.193
	05-06	9.917	-4.899	1.631	-0.196
	06-07	10.353	-5.194	1.662	-0.194
	07-08	10.723	-5.411	1.670	-0.189
	08-09	11.157	-5.731	1.708	-0.187
	09-10	11.635	-6.232	1.828	-0.195
	10-11	12.432	-6.883	1.986	-0.207
	11-12	12.933	-7.362	2.107	-0.216
	12-13	12.472	-7.041	2.016	-0.207
	13-14	12.747	-7.435	2.146	-0.221
	14-15	12.353	-7.016	2.014	-0.208
	15-16	12.274	-6.935	1.972	-0.202
	16-17	11.252	-5.849	1.644	-0.172
	17-18	10.280	-4.844	1.316	-0.139
	18-19	9.204	-3.832	1.049	-0.118
	19-20	7.502	-2.188	0.574	-0.076
	20-21	7.902	-2.895	0.936	-0.125
	21-22	8.017	-3.029	1.019	-0.136
	22-23	9.655	-4.873	1.694	-0.213
	23-24	9.317	-4.750	1.728	-0.222

TABLE 5. Coefficients of the polynomial fit to the quiet-time averaged fluxes

	LT	A_1	A_2	A_3	A_4
Protons	00-01	7.320	-3.510	0.921	-0.088
	01-02	6.940	-3.024	0.754	-0.071
	02-03	5.870	-1.929	0.403	-0.036
	03-04	3.723	0.409	-0.407	0.052
	04-05	3.763	0.542	-0.489	0.064
	05-06	3.676	0.654	-0.559	0.074
	06-07	3.167	1.298	-0.796	0.101
	07-08	3.013	1.471	-0.863	0.109
	08-09	2.191	2.263	-1.146	0.141
	09-10	2.162	2.394	-1.241	0.156
	10-11	3.172	1.498	-0.982	0.133
	11-12	4.185	0.441	-0.652	0.101
	12-13	5.321	-0.638	-0.327	0.070
	13-14	5.823	-1.311	-0.076	0.042
	14-15	6.801	-2.259	0.224	0.012
	15-16	7.725	-3.214	0.538	-0.021
	16-17	8.908	-4.422	0.941	-0.064
	17-18	10.456	-6.376	1.652	-0.142
	18-19	14.759	-10.447	2.881	-0.261
	19-20	11.019	-7.066	1.917	-0.173
	20-21	11.142	-7.057	1.900	-0.171
	21-22	12.464	-8.400	2.340	-0.217
	22-23	11.186	-7.218	2.013	-0.189
	23-24	10.579	-6.717	1.902	-0.183
Electrons	00-01	7.792	-2.927	1.024	-0.143
	01-02	7.819	-2.909	1.034	-0.145
	02-03	10.128	-5.308	1.831	-0.229
	03-04	10.820	-5.921	1.980	-0.239
	04-05	9.844	-4.765	1.549	-0.190
	05-06	10.087	-4.889	1.526	-0.181
	06-07	10.351	-5.035	1.538	-0.179
	07-08	10.425	-5.123	1.552	-0.179
	08-09	11.407	-5.994	1.767	-0.195
	09-10	11.479	-6.077	1.784	-0.196
	10-11	10.982	-5.663	1.645	-0.181
	11-12	10.768	-5.423	1.566	-0.172
	12-13	10.198	-4.988	1.428	-0.157
	13-14	10.624	-5.414	1.576	-0.173
	14-15	9.485	-4.155	1.166	-0.132
	15-16	9.341	-3.959	1.083	-0.122
	16-17	8.841	-3.423	0.922	-0.107
	17-18	9.632	-4.334	1.197	-0.132
	18-19	9.672	-4.462	1.262	-0.148
	19-20	8.769	-3.624	1.003	-0.115
	20-21	7.385	-2.216	0.585	-0.076
	21-22	5.714	-0.358	-0.008	-0.018
	22-23	7.789	-2.598	0.771	-0.101
	23-24	7.198	-2.161	0.697	-0.101

Table 6. Coeff. of the polynomial fit to the disturbed-time averaged fluxes

	LT	A_1	A_2	A_3	A_4
Protons	00-01	3.998	-0.421	0.052	-0.009
	01-02	4.907	-1.069	0.192	-0.018
	02-03	5.124	-1.207	0.233	-0.023
	03-04	3.512	0.248	-0.186	0.016
	04-05	4.547	-0.683	0.080	-0.009
	05-06	4.925	-0.979	0.171	-0.019
	06-07	5.178	-1.293	0.265	-0.027
	07-08	4.270	-0.291	-0.096	0.013
	08-09	2.429	1.568	-0.689	0.074
	09-10	2.101	2.134	-0.960	0.110
	10-11	2.266	2.162	-1.042	0.126
	11-12	3.836	0.729	-0.655	0.094
	12-13	6.634	-2.135	0.232	0.008
	13-14	8.968	-4.543	0.996	-0.069
	14-15	10.930	-6.562	1.671	-0.140
	15-16	11.609	-7.407	1.991	-0.177
	16-17	10.488	-6.137	1.588	-0.138
	17-18	7.322	-3.516	0.915	-0.083
	18-19	9.508	-5.596	1.534	-0.142
	19-20	8.326	-4.552	1.249	-0.118
	20-21	10.809	-6.988	2.029	-0.198
	21-22	7.234	-3.520	0.950	-0.090
	22-23	7.188	-3.414	0.910	-0.086
	23-24	5.663	-2.035	0.542	-0.056
Electrons	00-01	7.743	-3.213	1.274	-0.174
	01-02	6.978	-2.325	0.989	-0.146
	02-03	7.317	-2.457	0.961	-0.136
	03-04	6.893	-1.933	0.767	-0.113
	04-05	6.600	-1.734	0.721	-0.110
	05-06	7.241	-2.227	0.826	-0.117
	06-07	8.379	-3.233	1.084	-0.137
	07-08	8.391	-3.087	0.991	-0.123
	08-09	7.775	-2.314	0.684	-0.087
	09-10	9.107	-3.580	1.016	-0.115
	10-11	11.298	-5.575	1.570	-0.163
	11-12	12.412	-6.722	1.883	-0.190
	12-13	13.674	-8.249	2.383	-0.240
	13-14	14.368	-9.004	2.618	-0.264
	14-15	13.778	-8.469	2.444	-0.246
	15-16	13.343	-8.103	2.339	-0.237
	16-17	10.763	-5.344	1.474	-0.153
	17-18	8.474	-3.035	0.841	-0.103
	18-19	8.656	-3.469	1.108	-0.144
	19-20	8.655	-3.546	1.204	-0.162
	20-21	9.633	-4.922	1.763	-0.226
	21-22	9.343	-4.568	1.624	-0.205
	22-23	10.996	-6.438	2.321	-0.287
	23-24	9.675	-5.245	1.976	-0.254

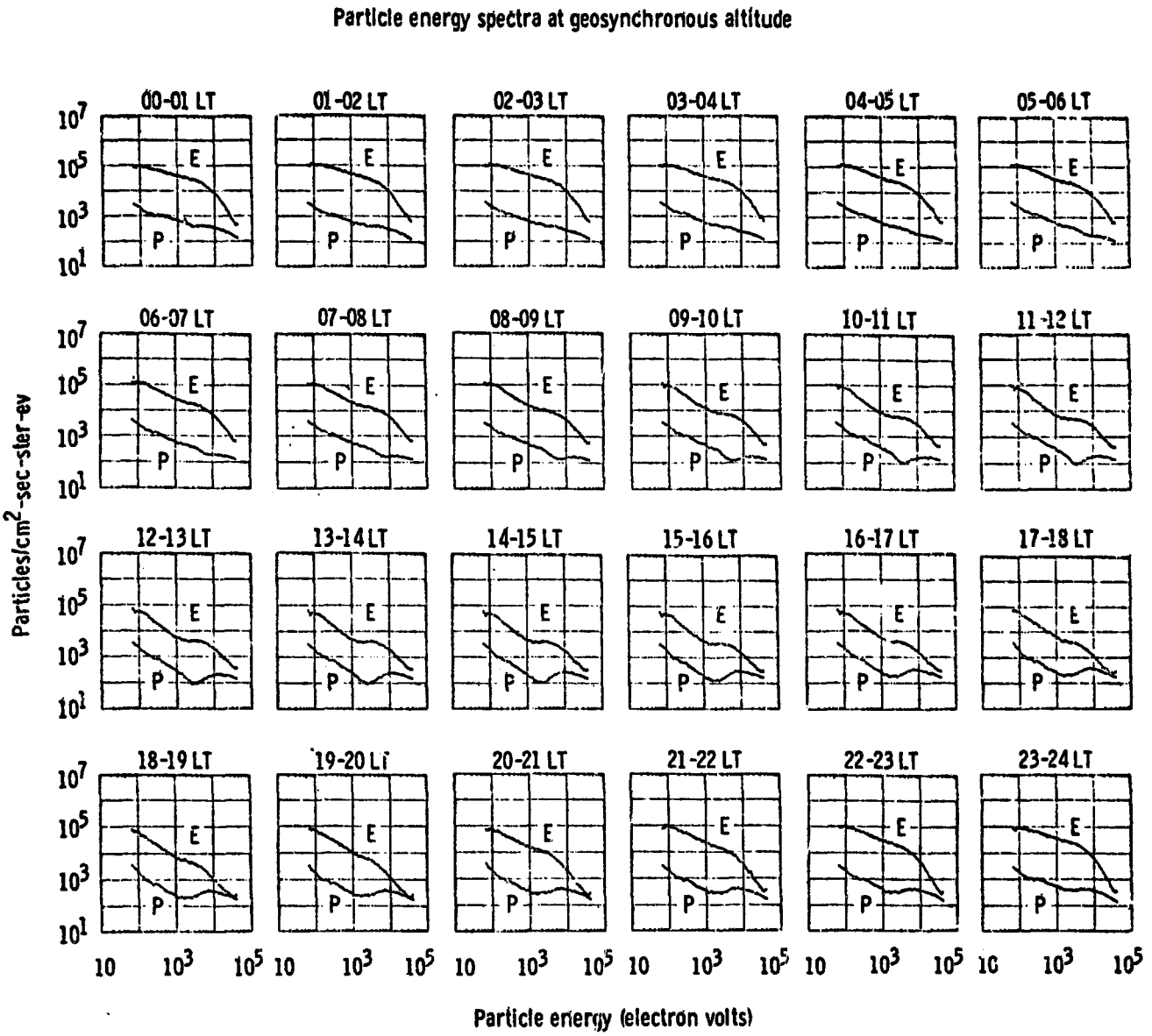

Figure 1: Hourly averages of the proton and electron fluxes observed by ATS-5 geostationary satellite in the year 1970. The upper curve in each frame is the electron flux intensity while the lower one is the proton flux intensity. Although the flux intensities between two adjacent local time observations are seen to be the same, great variations exists for flux intensities at widely separated locations.

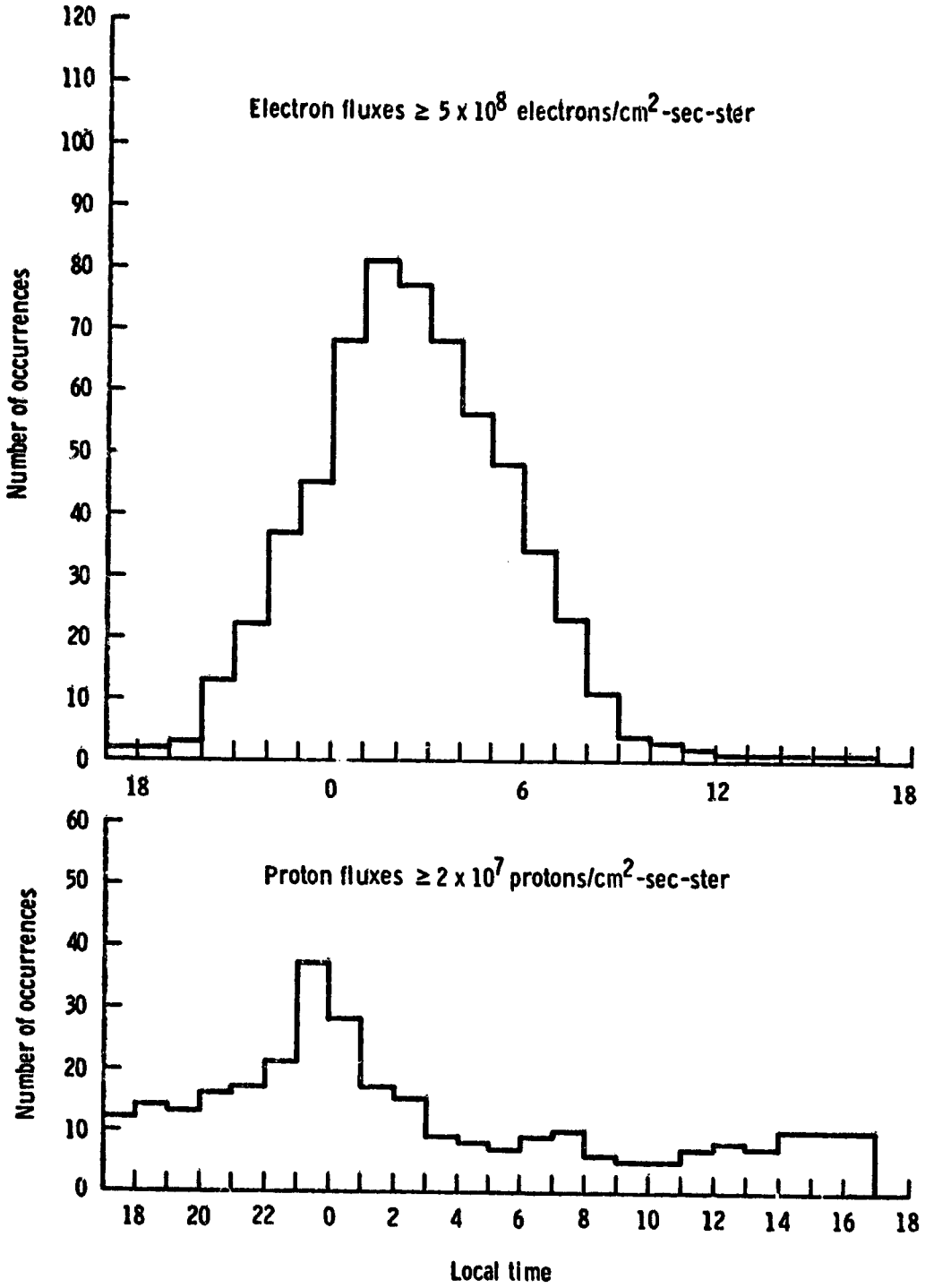

Figure 2: The frequency distribution of the occurrence of high flux intensities observed by ATS-5 in 1970. In general the high flux intensities were observed when the satellite was in the night-side magnetosphere.

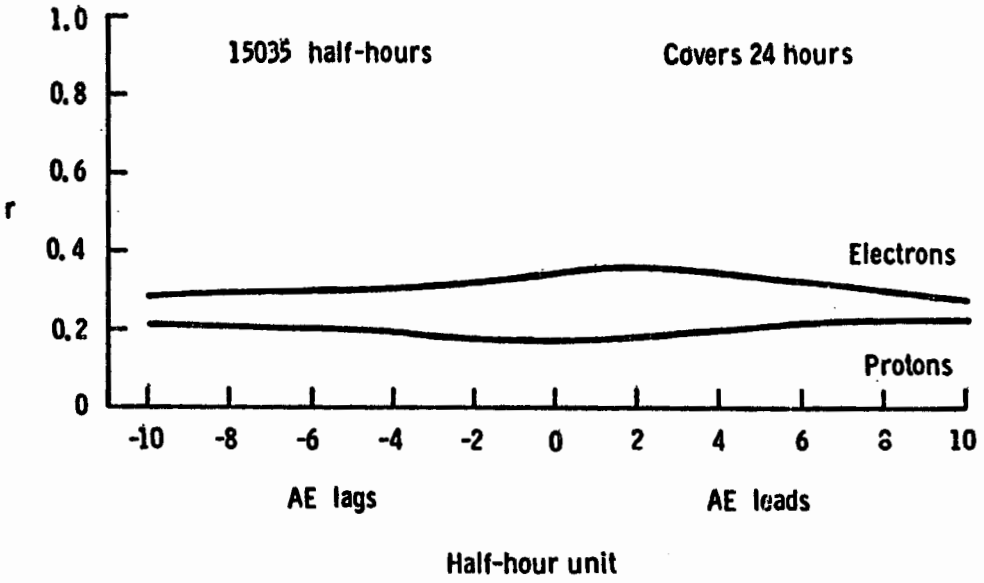

Figure 3: The linear correlation coefficients between the proton and electron flux intensities and the auroral electrojet (AE) indices at various lag times.

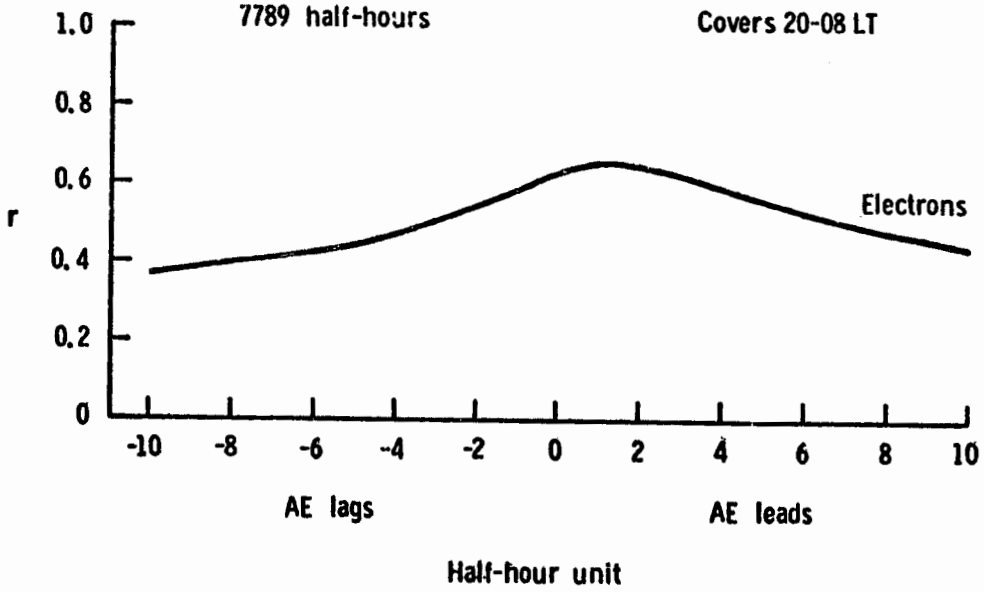

Figure 4: The linear correlation coefficients between the electron flux intensities observed by ATS-5 in the night-side magnetosphere and the AE indices at various lag times.